APPLIED PHYSICS LETTERS **104**, 121111 (2014)

CdS/PbSe heterojunction for high temperature mid-infrared photovoltaic detector applications

Binbin Weng,[1,a),b)] Jijun Qiu,[1,b)] Lihua Zhao,[1] Caleb Chang,[1] and Zhisheng Shi[1,2,a)]
[1]*The School of Electrical & Computer Engineering, University of Oklahoma, Norman, Oklahoma 73019, USA*
[2]*Nanolight, Inc., Norman, Oklahoma 73069, USA*

(Received 15 January 2014; accepted 16 March 2014; published online 27 March 2014)

n-CdS/p-PbSe heterojunction is investigated. A thin CdS film is deposited by chemical bath deposition on top of epitaxial PbSe film by molecular beam epitaxy on Silicon. Current-voltage measurements demonstrate very good junction characteristics with rectifying ratio of ∼178 and ideality factor of 1.79 at 300 K. Detectors made with such structure exhibit mid-infrared spectral photoresponse at room temperature. The peak responsivity R_λ and specific detectivity D^* are 0.055 A/W and 5.482×10^8 cm·Hz$^{1/2}$/W at $\lambda = 4.7\,\mu$m under zero-bias photovoltaic mode. Temperature-dependent photoresponse measurements show abnormal intensity variation below ∼200 K. Possible reasons for this phenomenon are also discussed. © *2014 AIP Publishing LLC*. [http://dx.doi.org/10.1063/1.4869752]

There is a strong market demand for uncooled photovoltaic (PV) detectors in mid-infrared (IR) wavelength range because cameras built with such detectors are much less expensive and more compact than cooled systems. Auger recombination is the major loss channel at high temperature for current semiconductor mid-IR detectors, and thus is the key hurdle for their development. Auger coefficient in Lead-salt (Pb-salt) materials[1,2] is more than an order of magnitude lower than those in type-II quantum wells (QWs),[3] which are in turn significantly suppressed relative to other III-V and II-VI semiconductors with the same energy band gaps. Recently, the uncooled PbSe photoconductive (PC) detectors have demonstrated significantly improved specific detectivity (D*) of 2.8×10^{10} cm·Hz$^{1/2}$/W (Ref. 4) and 4.2×10^{10} cm·Hz$^{1/2}$/W (Ref. 5) at ∼3.8 μm, without and with antireflective coating. However, in terms of Pb-salt PV detectors, this advantage of low Auger recombination has not been fully explored, which is partially due to lack of good junctions with low dark current.

Previous research works on Pb-salt PV detectors have been mainly focused on using Pb/Pb-salt Schottky junctions.[6,7] But the performance of such detectors is still far below the theoretical limit of Auger recombination. The performance enhancement is possible by the Pb-salt material quality improvement[8,9] or the device junction engineering. For the latter one, it has been shown that replacing Schottky contact by p-n homojunction can outperform their Schottky counterparts.[10–12] Furthermore, by constructing a larger band gap semiconductor with Pb-salt material to form p-n heterojunction with proper band offset will be able to offer even higher resistance-area product (R_0A) values by allowing minority carrier transport and blocking the majority carrier leak. Experimentally, however, due to the impurity inter-diffusion and other material related issues, the p-n homojunction mid-IR detectors have not been successfully developed. Therefore, finding a proper semiconductor material to form a good heterojunction with Pb-salts is critical for device performance improvement. It is worth mentioning that heterojunction based mid-IR Pb-salt PV detectors have not been explored yet.

CdS is a wide band gap semiconductor material with energy gap (Eg) at ∼2.4 eV and has been widely known as a n-type and window material in high efficiency thin film solar cells based on CdTe[13] and Cu(In, Ga)Se_2 (CIGS),[14] and other optoelectronic devices.[15] The electron affinity of CdS is around 4.5 eV,[16] which is close to PbSe material. Therefore, CdS has the potential to form a good heterojunction with PbSe film for mid-IR photodiode detector fabrication. In this letter, we report our research exploration on investigating the feasibility of using CdS/PbSe heterostructure for mid-IR detector applications.

The CdS/PbSe structure was prepared by two consecutive material growth procedures. First, PbSe thin film growth was performed on a 3-in. Si(111) substrate in a customized two-growth- chamber molecular beam epitaxy (MBE) system. The double polished high resistant Si wafer (∼3500 Ω·cm) was prepared by a modified Shiraki cleaning method[17] prior to the growth. After cleaning, the wafer was quickly dried by high purity N_2 gas purge and transferred into the MBE system. In order to obtain a high quality PbSe thin film on Si wafer with large lattice ($\Delta a/a = 12.7\%$) and thermal mismatches ($\Delta\alpha/\alpha = 646\%$), an ultrathin CaF_2 (∼2 nm) was grown in the first growth chamber as a buffer layer, because CaF_2 is nearly lattice matched to Si ($\Delta a/a = 0.6\%$) and has the thermal expansion coefficient ($19.1 \times 10^6\,K^{-1}$) near-perfectly matched with PbSe ($19.4 \times 10^6\,K^{-1}$) at 300 K. The substrate temperature during growth was controlled at 800 °C in order to obtain the 7×7 surface reconstruction of Si substrate for epitaxial growth of CaF_2. The PbSe film (1.2 μm) was then deposited in the second growth chamber. Substrate temperature was 390 °C for PbSe growth, and PbSe deposition rate was 25 nm/min. An additional Se source was used to adjust the p-type carrier concentration of the film and also to ensure the material quality due to the high Se vapor pressure during growth.

Second, CdS film was grown on top of the PbSe film by using chemical bath deposition (CBD) method. The PbSe

a)Electronic addresses: binbinweng@ou.edu and shi@ou.edu
b)B. Weng and J. Qiu contributed equally to this work.

 © 2014 AIP Publishing LLC

film on Si substrate was diced into 1×1 cm^2 small pieces prior to the CBD growth process. The small samples were fixed on a Teflon holder and kept vertically in the solution during growth. All chemicals used in the experiment were analytic grade reagents without further purification. A 15 ml mixed aqueous solution with $Cd(CH_3COO)_2$ (24 mmol) and NH_4CH_3COO (24 mmol) was used as Cd precursor, while a 15 ml thiourea (30 mmol) was used as sulfur precursor. These two solutions were mixed together in another 60 ml glass bottle and 7.5 ml $NH_3{\cdot}H_2O$ was introduced into the bottle as a complexing agent. Later on, PbSe samples in the Teflon holder were immersed in the aqueous solution, and the bottle was then heated up and stabilized for 1 h in the 60 °C water bath for subsequent CdS film (100 nm) deposition. After the growth, the as-grown CdS/PbSe samples were rinsed in deionized water and then purged to dry out under high purity N_2. In addition, CdS films grown under the same CBD procedure were prepared on pre-cleaned glass slides for material characterization.

The carrier concentrations of CdS and PbSe thin films prepared as the methods described above were determined to be $n \sim 1 \times 10^{16}\,cm^{-3}$ and $p \sim 3 \times 10^{17}\,cm^{-3}$, respectively, by Hall effect measurements in Van der Pauw four-point probe configuration, using fresh indium contacts, in an automated EGK HEM-2000 Hall Effect measurement system with a magnetic induction of 0.34 T. The electron concentration of CdS is over one order of magnitude lower than the hole concentration of PbSe at room temperature, which means that major depletion region would fall on the CdS side. Therefore, for the CdS/PbSe mid-IR detector structure in this paper, almost all of the photon-generated carriers in PbSe layers have to be collected through diffusion mechanism rather than quick drift process in the depletion region. Typically, the minority carrier lifetime in p-type PbSe grown on Si(111) is ~1 ns. Since the mobility measured through Hall effect is 500 $cm^2{\cdot}V^{-1}{\cdot}s^{-1}$ at room temperature, the diffusion length is calculated to be 0.928 μm from the equation $L_e = \sqrt{\mu k_B T \tau / q}$, in which L_e means the diffusion length, μ stands for the electron mobility, k_B is the Boltzmann constant, T is the absolute temperature, τ means the minority carrier lifetime, and q is the electron charge. Therefore, even most of the depletion region is in CdS layer, the photo-generated carriers are still sufficiently collected since the diffusion length is close to the thickness of PbSe film.

The fabrication process of the photovoltaic detectors starts with the 1×1 cm^2 as grown CdS/PbSe samples. The basic steps include: (a) definition of the area for PbSe exposure: Photolithographic patterning using AZ 2400 positive photoresist and MJB3 mask aligner, CdS etching using the diluted HCl etchant solution ($HCl{:}H_2O = 1{:}9$); (b) definition of the 200×200 μm^2 junction area using similar photolithographic technology and thermal vapor deposition of Au contacts for both CdS and PbSe layers. The metal contacts between Gold(Au)/CdS and Au/PbSe have been experimentally confirmed as ohmic type previously. Lift-off procedure was performed after the metal deposition; (c) mounting samples to test holders for temperature dependent measurements; For further testing purpose, the contacts on the device were wired up with the bonding pads with 20 μm Au wires using the Kulicke & Soffa 4523AD digital wedge bonder.

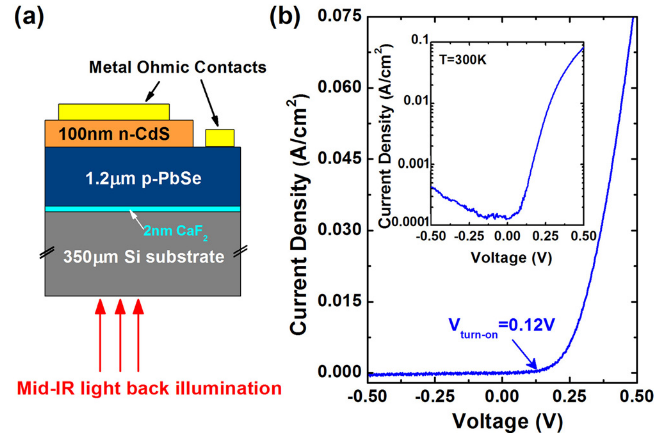

FIG. 1. (a) Configuration schematic of the CdS/PbSe heterojunction mid-IR photodiode; (b) Current density-voltage (J-V) characteristic of the diode from (a); the inset in (b) is the same J-V characteristic as (b) but with the current density in logarithm.

Figure 1 shows a schematic drawing of the CdS/PbSe heterojunction detector device's configuration and the room temperature dark current density versus voltage (J-V) characteristic of a 200×200 μm^2 n-CdS/p-PbSe heterojunction device performed by using Keithley 2400 source meter. By applying both reverse and forward bias from −0.5 to 0.5 V, it is clear that the heterojunction has a very good diode behavior according to the rectifying current flow through the junction as shown in the Fig. 1(b). The rectifying ratio measured at ±0.3 V is ~178. The dark current density is 1.15×10^{-4} A/cm^2 at −10 mV and a forward turn-on voltage is ~0.12 V. The forward J-V characteristic of a p-n junction can be described by the exponential relation $J \propto \exp(qV/\eta k_B T)$ when $\exp(qV/\eta k_B T) \gg 1$, V is the bias voltage, η is the ideality factor. Using the data from 0.15 to 0.25 V, η is determined by curve fitting to be 1.79, which indicates the recombination current may play a major role in this range. This together with the fact that dark currents increase with reverse-bias voltage, also reveal the presence of the interface imperfections that causes tunneling or leakage across the junction.

The detector performance was then evaluated by a detectivity measurement system. In this system, a calibrated 800 K blackbody from *Infrared System Development* is used as the standard infrared light source. A *Thorlabs* mechanical chopper is integrated in order to provide a frequency-modulated heat source. Photovoltaic mode is used which means zero bias is applied on the heterojunction diode during the measurement. Without connecting to any preamplifier, signal and noise currents from the device are directly collected by a *Stanford Research System SR830* lock-in amplifier. The responsivity R and specific detectivity D* are obtained by using the definition as shown below

$$\begin{cases} D^* = R \times \dfrac{\sqrt{A \times \Delta f}}{I_n} \quad (\mathrm{cm} \cdot \mathrm{Hz}^{1/2}/\mathrm{W}) \\ R = \dfrac{I_s}{P_i} \quad (\mathrm{A/W}) \end{cases}$$

where I_s and I_n are the measured detector output signal and noise currents, A is the device detection area, Δf is the noise bandwidth, and P_i is the incident radiant power. Peak

TABLE I. Performance characterizations of the CdS/PbSe photovoltaic detectors. (Note: λ_c is ~4.7 μm, and measurement is at photovoltaic mode (zero voltage)).

Detection area (μm^2)	T (K)	I_s (pA)	I_n (pA)	R at λ_c (A/W)	D* (λ_c, 700, 1 Hz) (cmHz$^{1/2}$/W)
200 × 200	300	500	2.0	0.055	5.482×10^8

responsivity R_{peak} and Peak detectivity D^*_{peak} are then calculated through a conversion factor defined in Ref. 18. Under 700 Hz chopping frequency modulation, the detector demonstrates R_{peak} of 0.055 A/W and D^*_{peak} of 5.482×10^8 cm·Hz$^{1/2}$/W at $\lambda = 4.7$ μm at 300 K under photovoltaic mode. Table I summarizes measurement conditions and results. It is noted that the cutoff wavelength λ_c is obtained from the spectral response measurement described as follows. This preliminary room temperature performance of the CdS/PbSe heterojunction detector implies its potential improvement through future optimizations in both structure design and material quality improvement.

Temperature-dependent mid-IR spectrum-resolved photoresponses of the CdS/PbSe heterojunction detector measured by Bruker IFS-66v Fourier Transform Infrared Spectroscope system are presented in Figure 2. The measurements were performed at temperatures ranging from 140 K to 320 K. As can be seen from Fig. 2(a), when temperature decreases from 320 K to 200 K, both photoresponse and the cutoff wavelength increase gradually. After the temperature drops below 200 K, the cutoff wavelength is still increasing with the decreasing temperature, but the peak photoresponse intensity decreases as illustrated in Fig. 2(b), which is an abnormal performance behavior. To make it clear, the peak photoresponse intensities and the cutoff wavelengths are plotted versus the temperatures in Figure 3. Apparently, the maximum photoresponse intensity is obtained at around 200 K.

In order to understand the response intensity behavior of the detector with the temperature, first of all, we need to discuss the quantum efficiency of the CdS/PbSe photodetector. There are two regions in PbSe layer that produce photo-generated carriers, including neutral p-type region and junction region on PbSe side. In this back illumination case, the incident light intensity decays exponentially in the PbSe layer (1.2 μm) and thus most of photo-generated carriers are in neutral p-type PbSe region. On the other hand, as mentioned previously, due to carrier concentration difference, most of the depletion region drops in CdS side. The calculated depletion width in PbSe side at room temperature is only ~ 2.7 nm. Although depletion width will change with temperature, it is still insignificant compared to the PbSe film thickness. And due to the zero bias photovoltaic mode operation method, the carrier collection efficiency affected by bias condition is not a factor to be considered in this case. As a result, photo-generated carriers in neutral p-type PbSe region dominate the photodetector quantum efficiency which can be described as follows, assuming there is no potential barrier for minority carrier transport due to heterojunction band offset[19]

$$\eta_p = \frac{(1-r)\alpha L_e}{\alpha^2 L_e^2 - 1}\left\{\frac{\alpha L_e - e^{-\alpha x_p} sh(x_p/L_e)}{ch(x_p/L_e)} - \alpha L_e e^{-\alpha x_p}\right\},$$

in which r is the illuminated junction surface reflection coefficient, α is the absorption coefficient, L_e is the electron diffusion length as mentioned, and x_p is the distance from backside of PbSe film to the p side junction boundary. Therefore, it is clear that the temperature dependent parameters including diffusion length L_e and absorption coefficient α play major parts in affecting the quantum efficiency and eventually photoresponse. As stated above, diffusion length $L_e = \sqrt{\mu k_B T \tau / q}$. Carrier mobility in lead-salt semiconductor is proportionally to $T^{-5/2}$ mainly due to the decrease of phonon scattering.[20] On the other hand, it is known that minority carrier lifetime, especially at lower temperatures, in PbSe film is dominated by the Shockley-Rheed-Hall (SRH) recombination process which is barely affected by temperature. Therefore, diffusion length increases at lower temperature. The absorption coefficient of PbSe material can be calculated based on the theory described in Ref. 21. From the calculation, not only the absorption edge red-shifts to longer wavelength, but also the absorption coefficient increases slightly in the photoresponse spectral range at lower temperature. Therefore, temperature-dependent quantum efficiency can be estimated by using the discussed diffusion length and absorption parameters. Our simulation based on the theory

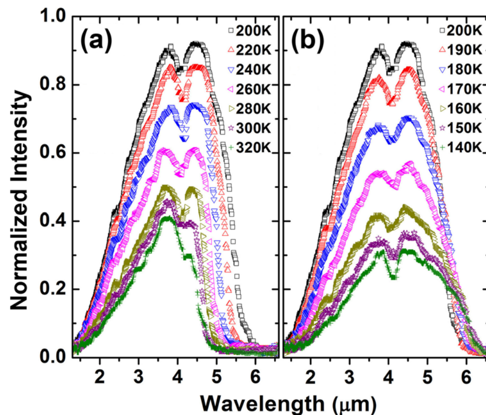

FIG. 2. Temperature dependent photoresponse of the CdS/PbSe heterojunction mid-IR photodiode (a) from 320 K to 200 K; and (b) from 200 K to 140 K.

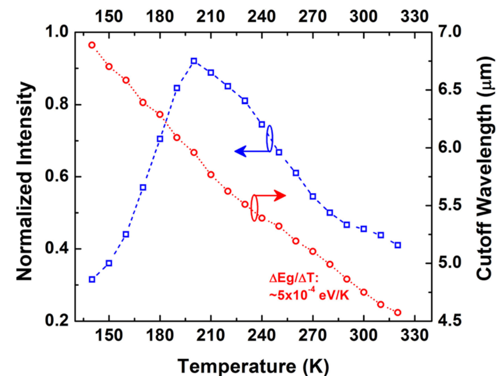

FIG. 3. Normalized peak photoresponse intensity (in red circle dotted line) and the cutoff wavelength (in blue square dashed line) of the CdS/PbSe mid-IR detector with temperature.

described above shows that quantum efficiency unidirectionally increases from ~20% to ~70% while temperature drops from room temperature down to ~140 K. As a result, the photoresponse intensity should typically increase at lower temperature, which explains Fig. 2(a).

Therefore, the abnormal decrease of photoresponse intensity below 200 K must be caused by other mechanisms. Here, we provide one possible qualitative explanation. It is known that the electron affinities of these two materials are near 4.5 eV at room temperature.[16,24] As temperature decreases, energy barrier might form due to the variation of the CdS/PbSe band offset, as marked in Figure 4(b). Energy band gap of PbSe has a positive temperature coefficient, which means the band gap reduces at lower temperature.[22] This is also observed in our temperature-dependent cutoff wavelength variation, as shown in Fig. 3. The temperature coefficient for PbSe measured is about 5×10^4 eV/K, which agrees with Ref. 22. CdS energy band gap, on the other hand, has a negative temperature coefficient. The temperature dependent energy band gap of CdS can be expressed as[23]

$$Eg(T) = 2.5825 - 3.06 \times 10^{-3} \times T^2/(2156 + T).$$

Estimated temperature coefficient from this equation is about -5×10^4 eV/K. If thermal excitation is ignored, the band alignment should be type II as is shown in Fig. 4(a) to allow electron transport from p-PbSe to n-CdS, so that photoresponse could be observed and increases while temperature decreases. However, as the temperature drops, the energy band gap of PbSe decreases while CdS band gap increases. When the temperature is below 200 K, the band alignment might shift to type I (the PbSe bandgap is in-between the CdS bandgap), as shown in Fig. 4. Consequently, presence of the barrier resulting from the change of conduction band offset (ΔE_c) could gradually limits the diffusion of photo-generated electrons by a factor of $e^{-\frac{q\Delta E_c}{k_B T}}$,[25] and thus photoresponse could start to drop even though the quantum efficiency affected by other parameters in PbSe layer still increases as discussed before. In addition, we also noted that possible temperature-dependent changes at CdS/PbSe interface such as interface states caused by, e.g., mismatch of thermal expansion coefficient could also affect the device performance. Lack of information on such interface states and other temperature-dependent material parameters of polycrystalline CdS make it difficult for us to address such possibility, especially quantitatively. Future work on temperature-dependent band offset using other methods, and on polycrystalline CdS/MBE-PbSe interface and other material parameters could help further clarify this abnormal behavior. Nevertheless, the results demonstrated in this work have proved the feasibility of using CdS/PbSe heterostructure for mid-IR detection at high temperatures.

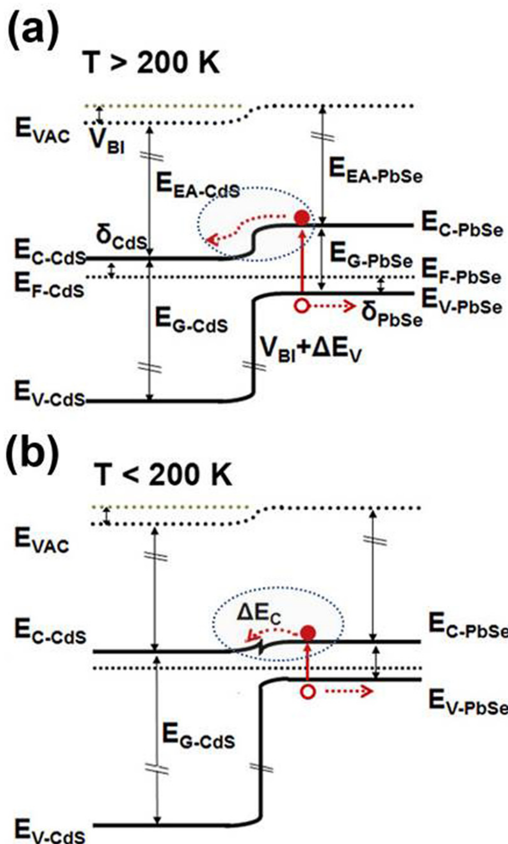

FIG. 4. (a) Suggested energy band diagram of the n-CdS /p-PbSe heterojunction at (a) above 200 K and (b) below 200 K. (In the figure, E_{vac}, E_C, E_F, E_V, E_{EA}, V_{BI}, E_G, ΔE_V, δ stands for vacuum energy, conduction band energy, Fermi energy, valence band energy, electron affinity, built-in potential, energy band gap, valence band offset, and energy difference between Fermi energy and conduction band, or Fermi energy between valence band, respectively)

In conclusion, CdS/PbSe n-p heterojunction mid-IR photodiodes are proposed and fabricated in this work. The device exhibits good I-V characteristics and photoresponse at room temperature. Spectral photoresponse measurements demonstrate a promising potential of using CdS/PbSe heterojunction for mid-IR detection applications. In addition, temperature-dependent mid-IR spectral response performance showed an abnormal performance decrease below 200 K, it is suggested that band alignment transition could be a possible cause for the phenomenon. We anticipate significant device performance enhancement through material parameters optimization, which could eventually lead to uncooled PV mid-IR detectors with high detectivity.

We acknowledge financial supports from the DoD AFOSR under Grant No. FA9550-12-1-0451, DoD ARO Grant No. W911NF-07-1-0587, and Oklahoma OCAST program under Grant Nos. AR112-18 and AR132-003.

[1]R. Klann, T. Hofer, R. Buhleier, T. Elsaesser, and J. W. Tomm, J. Appl. Phys. **77**, 277 (1995).
[2]P. C. Findlay, C. R. Pidgeon, R. Kotitschke, A. Hollingworth, B. N. Murdin, C. J. G. M. Langerak, A. F. G. van der Meer, C. M. Ciesla, J. Oswald, A. Homer *et al.*, Phys. Rev. B **58**, 12908 (1998).
[3]J. R. Meyer, C. L. Felix, W. W. Bewley, I. Vurgaftman, E. H. Aifer, L. J. Olafsen, J. R. Lindle, C. A. Hoffman, M.-J. Yang, and B. R. Bennett *et al.*, Appl. Phys. Lett. **73**, 2857 (1998).
[4]J. Qiu, B. Weng, Z. Yuan, and Z. Shi, J. Appl. Phys. **113**, 103102 (2013).
[5]B. Weng, J. Qiu, Z. Yuan, P. Larson, G. Strout, and Z. Shi, Appl. Phys. Lett. **104**, 021109 (2014).
[6]D. K. Hohnke and H. Holloway, Appl. Phys. Lett. **24**, 633 (1974).
[7]H. Zogg, A. Fach, J. John, J. Masek, P. Muller, C. Paglino, and S. Blunier, Opt. Eng. **34**, 1964–1969 (1995).
[8]P. Muller, H. Zogg, A. Fach, J. John, C. Paglino, A. N. Tiwari, and M. Krejci, Phys. Rev. Lett. **78**, 3007–3010 (1997).
[9]B. Weng, F. Zhao, J. Ma, G. Yu, J. Xu, and Z. Shi, Appl. Phys. Lett. **96**, 251911 (2010).

[10]S. C. Gupta, B. L. Sharma, and V. V. Agashi, Infrared Phys. **19**, 545–548 (1979).
[11]H. Preier, Infrared Phys. **18**, 43–46 (1978).
[12]H. Zogg, A. Fach, C. Maissen, J. Masek, and S. Blunier, Opt. Eng. **33**, 1440–1449 (1994).
[13]C. S. Ferekides, D. Marinskiy, V. Viswanathan, B. Tetali, V. Palekis, P. Selvaraj, and D. L. Morel, Thin Solid Films **361–362**, 520–526 (2000).
[14]K. Orgassa, U. Rau, Q. Nguyen, H. W. Schock, and J. H. Werner, Prog. Photovoltaics **10**, 457–463 (2002).
[15]N. Sfina, N. Zeiri, A.-B. Nasrallah, and M. Said, Mater. Sci. Semicond. Process. **19**, 83–88 (2014).
[16]L. E. Brus, J. Chem. Phys. **79**, 5566 (1983).
[17]H. Okumura, T. Akane, Y. Tsubo, and S. Matsumoto, J. Electrochem. Soc. **144**, 3765–3768 (1997).
[18]E. L. Dereniak and G. D. Boreman, *Infrared Detectors and Systems* (John Wiley & Sons, New York, 1996), p. 208.
[19]A. Rogalski and J. Rutkowski, Infrared Phys. **22**, 199–208 (1982).
[20]Yu. I. Ravich, B. A. Efimova, and V. I. Tamarchenko, Phys. Status Solidi B **43**, 453 (1971).
[21]O. Ziep and D. Genzow, Phys. Status Solidi B **96**, 359–368 (1979).
[22]A. Katzir, R. Rosman, Y. Shani, K. H. Bachem, H. Bottner, and H. M. Perier, in *Handbook of Solid State Lasers*, edited by P. K. Cheo (Marcel Dekker, New York, 1989), pp. 227–347.
[23]Y. P. Varshni, Physica **34**, 149 (1967).
[24]X. Jiang, R. D. Schaller, S. B. Lee, J. M. Pietryga, V. I. Klimov, and A. A. Zakhidov, J. Mater. Res. **22**, 2204 (2007).
[25]J. H. Werner and H. H. Guttler, J. Appl. Phys. **69**, 1522 (1991).